Enzyme Catalytic Activity Emulated Within DNA-based Nanodevice

Tadija Kekić, Yasaman Ahmadi and Ivan Barišić[1]
Molecular Diagnostics, Center for Health and Bioresources, AIT Austrian Institute of Technology GmbH, Giefinggasse 4, 1210 Vienna, Austria

[1]Corresponding author. Email: Ivan.Barisic@ait.ac.at

ABSTRACT

Artificial enzymes hold great potential in the field of biotechnology. We present an approach towards the bottom-up development of an artificial enzyme using the DNA origami technology. A set of peptide-oligonucleotide conjugates, designed to recreate the structure of an active site of a native protein, was placed in the central area of a large, self-folding DNA origami shell structure. The peptide-oligonucleotide conjugates were placed in a predefined positions by the integration on the angle-adjustable, linear constructs that protruded from the nanostructure. We demonstrate a workflow to obtain the essential elements of the protein's active site; to design and assemble the nanodevice; to measure, quantify and inactivate the catalytic activity; and to reuse our structures in multiple experiments. By use of the high-resolution spectroscopy, we demonstrated a significant increase in the product accumulation that originates from the correctly assembled emulated active sites.

Introduction

The functionalisation of nanodevices presents a serious challenge in the field of nanotechnology and is often inspired by the existing solutions found in nature. To achieve its function, a state of the art nanodevice employs binding of enzymes [1,2,3], fluorophores [3,4,5,6], antibodies [7,8], aptamers [5,8,9] and other active elements [12,38], while nanostructures itself act as a scaffold for the organisational purposes. Biological solutions however, are not easily implemented. To function properly, they require a specific environment, interaction with partners, correct phosphorylation and glycolisation profiles [10,11,19]. Enzymatic catalysis of a chemical reaction is an example of biological efficiency. Due to the isolation difficulties of the enzyme, the scarcity of the available catalysts, of many important chemical reactions, creates production bottlenecks in diagnostics and industry [20]. As such, development of artificial systems with catalytic properties is a lasting challenge.

Over the last decade, DNA emerged as a versatile material for generating highly complex nanostructures of unprecedented precision, by the implementation of DNA-origami technologies [13,14,15]. The maturation of these technologies, together with the available software packages reached the state that allows development of nanostructures with novel functions and properties [16,17,18]. In the same time, the field of artificial enzymes attracted attention with several prominent publications on the *de novo design* of the catalytic systems [20-25]. Although, experimental approach, size and complexity between described systems significantly varied, they have mutual design principles, as the artificial catalytic properties are based on the introduction of modifications, on predefined positions, in a stable framework structure.

To maintain the stability of the active site, the structures of artificial enzymes are often based on extremely conserved proteins with stable secondary or tertiary structures [20, 25]. When directly connected to this type of framework, the stability of the artificial catalytic site is increased, however, the design of the active site becomes limited. The framework structure, of a top-down design approach, allows for only a small number of designated places for the positioning of the key functional groups [20,23,25]. Further, introduction of the mutations in the peptide sequence can affect protein folding, and destabilise or structurally change the whole construct, and not only the functional groups involved in the artificial catalytic process.

In this study, we demonstrate an implementation of a bottom-up approach in emulating catalytic properties of an arbitrary enzyme *de novo*, in an artificial nanodevice.

As a proof of concept, we designed a nanodevice capable of emulating ATP hydrolysis, a fundamental biological reaction often associated with the energy transfer to the proteins with motoric functions. The emulation of the ATPase activity was based primarily on the FlaI protein complex from *Sulfolobus acidocaldarius*, the simplest, transmembrane and motoric supracomplex *[19,26]*. ATP hydrolysis in the FlaI, accompanied by the domain movements in the complex generates a torque, a rotational force that is channelled through the filament of the transmembrane protein supercomplex of the archellum [19, 26]. The FlaI-like ability to efficiently transform the chemical to mechanical energy is becoming exceedingly important, as the emulation of this property is a step towards development of the power supply units with various nanomechanical purposes [27, 28]. This FlaI was also chosen as it meets other selection criteria, such as the elucidated crystal structure, a well-defined and open active site, available reaction kinetics data and a established colorimetric assay for tracing the accumulation of the products [19, 26, and 29].

RESULTS

Analysis of FlaI protein complex

The crystal structure of the FlaI hexamer (PDB: 4II7) was used to generate the protein complex systems *in silico* [19]. Domain dynamics and the interactions between the enzyme's active site, the substrate, the products and the cofactor were analysed using the molecular dynamics (MD) simulations (Fig. 1). Due to the highly dynamic nature of the FlaI hexamer, we observed significant deviations in both conformations and relative positions of amino acids in the active site. The analysis of the MD simulations and the available quantum mechanics data from similar systems [30 - 34] helped identifying and investigating the key amino acids, which are both structurally and catalytically important (Fig. 1). The amino acids were further selected by the phylogenetic and structural comparison of data available from the homologous proteins, exhibiting the total sequence similarities above 90%. Based on their role in the interaction with the substrate, the products and the cofactor, the key, conserved amino acids were assigned to groups (Fig. 1). The first group provided for the binding capabilities of the active site which was predominantly located in the surrounding area of the nucleotide base and deoxyribose sugar. The second group resembled the environment surrounding the phosphate groups, thus being more directly involved in the catalytic process. The third group was purposed to stabilise the metallic ion in the proximity of gamma phosphate group.

Design of emulated catalytic site

The obtained structural data was used for *in silico* modelling of a small, base level DNA Scaffold Embedded Protein Emulation Complex or D-SEPEC. The base structure was retroactively expanded through a systematic addition of the neighbouring amino acids, while keeping the elements of D-SEPEC close to the steric and electrostatic energy minimum. Throughout this process amino acids conformation were adjusted from the one found in the crystal structure of the native protein, and in some cases residue-type of amino acids was changed. However, amino acids retained similar functional properties with respect to the difference in the environment, and their interactions within the active site. Further key amino acids modifications were done in order to enhance the stability of binding interactions between the substrate and active site, and to adjust the residues involved in the hydrophobic interactions previously utilized in forming the tertiary structure of the original protein. The expanded, proximal amino acids were joined by the peptide bonds until four oligopeptides, 10 – 15 amino acids in length, were formed.A total of 46 amino acids from the FlaI protein were used. The model was further expanded by addition of four oligonucleotides, each having a single base modified into the 5-ethynyl-2'deoxyuridine. Similarly, the appropriate amino acids in each oligopeptide were modified into the L-azidohomoalanine linker, rendering them capable of click chemistry reaction with their oligonucleotide counterparts. In this way, four peptide-oligonucleotide conjugates (POC) were formed, each representing one element of the emulated active site (Fig. 1). The newly formed interactions between the oligopeptides and the oligonucleotides were closely monitored, and further modifications to the D-SEPEC were made to minimize the effect that a newly-introduced, negatively charged DNA oligonucleotides exhibited on the emulated active site.

D-SEPEC integration into a nanostructure

To maintain the relative position and the orientation of D-SEPEC elements, a sturdy, DNA – origami based, hexagonal prism, named „the Shell" was designed (Fig. 1). D-SEPEC was placed in the central position in the Shell structure. To connect D-SEPEC to the Shell, each POC was embedded in the 20 nucleotides long, ssDNA Carrier strand element (Fig. 1, f). The projective lines, emanating from the short Carrier strand elements were calculated, and used to align D-SEPEC - Carrier strands superstructure towards the optimal, Shell's inward-facing staple strands. To reach Shell, the Carrier strands were linearly elongated. To integrate them, the ends of the Carrier strands were extended into the appropriate DNA staple strand (Fig. 1, g). In this way, the D-SEPEC elements are kept in a stable position relative to each other (via Carrier strands), in the central area of the nanodevice, with a minimised interaction between the POC elements and the bulk of the Shell and Carrier structures (Fig. 1,h). Once the complete model of D-SEPEC nanodevice was created, the sequences of POCs oligonucleotides and staple strands were calculated and checked for any unspecific binding, hairpins, self/hetero-dimers, as well as for the acceptable length, binding strength and melting temperature [44].

Structural properties of D-SEPEC nanodevice

As confirmed by the TEM imaging and agarose gel electrophoresis (Fig. 1, j), D-SEPEC nanodevice is a large, rigid and roughly hexagonally shaped DNA-based nanostructure, assembled from 500 DNA elements. It was comprised of 15624 bp of the Shell's elements, 500 bp of the Carrier strands elements, and 80 nucleotides linked to 46 amino acids of the POC elements. The molecular weight of the nanostructure was approximately 5339 kDa. The height of the hollow Shell structure was approximately 45.8 nm, with the width ranging from 43.4 nm to 46.26 nm. The distance between D-SEPEC and the bulk area of the Shell structure was approximately 17.0 nm. The solvent accessible surface area of the nanostructure was approximately 44870.1 nm3, with peptide area of only 3.3 nm3.

Catalytic Activity Assay

We performed a series of tests to determine the catalytic potential of D-SEPEC nanodevice (Fig. 2). It was designed with the purpose to catalyse the exergonic hydrolysis of ATP in the reaction that generates ADP and inorganic phosphate (PO_4^{3-}). The phosphate accumulation speed was measured using the Malachite Green Phosphate assay kit (Sigma-Aldrich). Once complexed with a free orthophosphate, the malachite green molybdate (yellow) forms the molybdophosphoric acid (green), which has an absorption maximum in the area between 620 and 640 nm. As the absorbance in this wavelength interval directly correlates with the concentration of the generated orthophosphate, the standardised orthophosphate gradients were used to quantify the turnover rate of the catalytic reactions. Following the assembly, the reactions were initiated by addition of 0, 25 or 50 μM of ATP to the pools of test and control nanostructures and buffers. The samples were incubated for a period of up to 24 hours at room temperature, while shaking (at 300 rpm). In the initial experiments, a direct addition of the malachite green reagents to the reaction mixtures resulted in the formation of a visible aggregate that significantly affected the reliability of measurements. To solve the aggregation problem, in the following experiments we performed ultrafiltration of the samples using the 5 kDa ultrafiltration system, before the addition of the malachite reagents. The nanostructures and smaller DNA elements as the POC and the Filler pools thus remained in a small retention volume, while the free orthophosphates, ADP and ATP were harvested within the flow through and analysed by a high-resolution spectroscopy.

Inactivation of the catalytic activity

To confirm that the presence as well as the correct positioning of a D-SEPEC elements are both the essential factors of the emulated catalytic activity, we designed two inactivation experiments. The first inactivation experiment used the Fillers, the oligonucleotide equivalents of the POC molecules, in construction of the non-functional D-SEPEC nanodevices. The Fillers were added during the process of super assembly, and they were designed as the catalytically inactive replacement for the POC molecules, with the same relative angles as in the correctly assembled nanostructure. The goal of this experiment was two-fold: first, we wanted to determine if the catalytic properties of the nanostructure originate from the POC, or from the DNA elements of nanostructure; second, by creating a structure entirely made of DNA, we wanted to measure the effect that the natural degradation and/or possible DNAzyme sequences inside of the large DNA-based nanostructure might have on the effectiveness and the resolution of the malachite green assay.

In the second type of the inactivation experiments, the pools of fully assembled D-SEPEC nanodevice were incubated at 95 °C for 15 minutes, and cooled down to the RT. This resulted in denaturation of the whole nanostructure, followed by its reassembly into the aggregates of low specificity. Following the cooling and aggregation of the samples, the reactions were initiated by addition of the substrate, and the incubation for up to 24 hours. The goal of this experiment was to test if the random and unspecific interaction between the DNA and POC molecules will affect the product generation speed in comparison to the correctly assembled D-SEPEC nanodevice. The construction of the Test and the Control nanostructures followed the same assembly and purification steps, while the PEG purification steps in the preparation of Fillers and POCs pools controls were performed by the supplier, IDT.inc for oligonucleotides, and Biomers.net for custom POCs (Fig. 2).

Product accumulation analysis

Due to the effect that a prolonged incubation with malachite green has on the hydrolysis of ATP, the assays were conducted as the endpoint measurements of the product concentrations. All test and control experiments were repeated 110 times, with five incubation intervals of 0, 6, 12, 18 and 24 hours. The final concentration of ATP in each sample type was 0, 25 or 50 μM. In each experiment, all test and control reactions were performed in four replicates, with an exception of the substrate-free control samples, which were measured in triplicates. Each sample was measured 10 times within several seconds. The data were analyzed by comparing the median values of the combined measurements of all replicates of each sample type at the same incubation interval. The general medians were calculated from all 110 experiments. The samples were blanked by the absorption values of malachite green reagents in a control buffer with no ATP added, with the absorbance values in the range of the control reactions of malachite green reagent and MiliQ water. The sample type dependent product generation is shown in Figure 2, where each data point represents a median and standard error of approximately 4400 measurements, taken across the 440 reactions of ATP hydrolysis.

Based on the differences of the product accumulation between sample types, several observations have been made. In the control samples with no ATP, during the incubation period of 24 hours, the absorbance of the malachite green reagent was minimally changed. A slight an increase was observed in sample types which contained the Shell structure, the biggest structural element of the nanodevice. The absorbance increase observed in the substrate-free controls could be explained by the experimental artefacts, such as the passive rise of the PO_4^{3-} concentration caused by the slow degradation of the DNA-based nanostructures, or less likely, complexation of malachite green reagent with the nanostructures. Although unexpected, the absorbance increase observed in this group of control reactions was shown to be minimal, in contrast to the test reactions with the added substrate.

In reactions with the added 25 µM ATP substrate, a slow increase of the PO_4^{3-} concentration detected in buffer control samples indicated a natural degradation of ATP occurs under given conditions. As such, the buffer control measurements were used as a baseline in determining the change in the product generation speed. A low rate of the product accumulation was also observed in the control samples of both POC pools, and Filler pools. Similarly to the Filler oligonucleotides, the POC molecules, consisting of both the peptide and the oligonucleotide parts, can unspecifically interact with each other, forming the aggregates of amorphous structure. As the product accumulation in control samples of POC pools was comparable to that observed as a result of the passive autohydrolisation of ATP, this suggested that the random combinations of POC molecules were unable to catalyse the hydrolysis of the substrate. Further, it confirmed that the Filler molecules do not contain DNAnzyme sequences.

In control reactions using the correctly assembled, non-functional nanodevices made from Shell, Carrier and Filler elements, we observed a strong decrease in the product accumulation (k_{cat} = 0.0567– 0.1361 s^{-1}), when compared to the samples containing the D-SEPEC nanodevices. In contrast to the buffer controls, as well as the substrate-free controls of the same type, the observed values were significantly higher. The product accumulation in the samples containing the non-functional nanodevices indicated that some level of interaction exists between the DNA-based superstructure and the ATP substrate. Due to the high amount of the staple strands used in a construction of the nanodevice, we could not completely eliminate a possibility that some of them might possess a certain capacity to hydrolyse ATP, or to interact with malachite green. As the observed product increase was relatively low when compared to the active D-SEPEC, (k_{cat} = 0.2271 – 0.3622 s^{-1}), it is more likely that the DNA-based superstructure exerted a pasive influence on its microenvironment, affecting the stability of the surrounding ATP molecules and making them more susceptible to autohydrolysis. The product accumulation of the Shell-Carrier-Filler samples were used to correct the turnover speed calculations of the active centre in a D-SEPEC nanodevice.

Heat denaturation was used to destabilise the correctly assembled, functional D-SEPEC nanodevice. By heating the samples to 95 °C and cooling them to room temperature prior to the addition of the substrate, we significantly hindered the generation of the product in reactions with the D-SEPEC nanodevice, (k_{cat} = 0.1114– 0.1253 s^{-1}). This suggests that the POC elements of the active centre will be able to hydrolase ATP only when correctly assembled. As the heat denaturation of the samples brought the product generation levels close to those observed in the Shell-Carrier-Filler reactions, we expect that the DNA used in the construction of the nanodevice has some influence on the ATP hydrolysis.

The catalytic properties of D-SEPEC nanodevice built in three separate, start to finish, assembly processes were analysed in a total of 1330 reactions, spread over sample types named D-SEPEC 1, 2 and 3 (Fig 2). In comparison to the buffer controls, test reactions of D-SEPEC nanodevice consistently exhibited the strongest increase in the product accumulation levels. The measurements were converted to the $PO43^-$ concentrations by corelating them with the absorption of the orthophosphate standards in the concentration gradient. After subtracting the values attributed to the observed influence of the Shell structure, we approximated the turnover rate of the D-SEPEC nanodevice to be in the range of 1 to 20 ATP molecules per unit of D-SEPEC per minute of incubation on the RT (see Fig. 2). Recent studies on the isolated *Sulfolobus's* FlaI reported the turnover rate of the enzyme to be around 1 ATP per unit of enzyme per minute, making it slower than D-SEPEC nanodevice [19]. A similar turnover speed was noted in the reactions where 50 µM ATP was used for the incubation, with the effect that the increase of the substrate concentration led to the higher coherence of measurements between the D-SEPEC sample types made by separate assemblies (Fig. 2).

DISCUSSION

Demand for the mass production of the enzymes, required for their ability to efficiently catalyse a chemical reaction, led to the developments of several successful strategies for the recreation of the catalytic properties in the rationally designed constructs[1 -3, 20 – 22, 35 - 37]. One of the most implemented approaches is the bonding and compartmentalisation of one or more enzymes on a surface of a nanostructure. Wilner et al. (2009) demonstrate how a topological placement on the DNA-based framework can be used to regulate the activity of the enzymatic systems. Linko et al. (2015) proposed an enzyme cascade nanoreactor to increase the catalytic activity of enzyme pair, while Grossi et al. (2017) developed nano-containers with programmable structural dynamics capable of regulating the enzyme-substrate interaction. The activity of the enzymes bonded with the nanostructures varies from native to several times higher activity [35, 36]. However, use of the native enzymes in creating of a functional nanostructure has two main limitations. First, the turnover speed is limited by the biology of the enzyme, thus slower enzymes require an alternative strategy. Second, the approach is restricted to the use of enzymes we are able to express and purify in a form that will retaining its function once it is attached to the nanostructure.

Rothlisberger et al. (2008), presented an approach for a bottom up design of a protein structure capable of catalysing the reaction of Kemp elimination. In their work, an idealized active site comprising several amino acids was modelled and encoded into the tertiary structure of the TIM barrel, one of the most conserved structural domain of many enzymes. To improve the computationally designed model, *in vitro* evolution methods were implemented resulting in increased stability, expression and activity of the artificial enzyme. Rothlisberger et al. noted that the most beneficial *in silico* modifications were made on the residues adjacent to the key catalytic amino acids, as a form of fine tuning the shape of the active site. The reported catalytic rate

constant (k_{cat}) of the artificial enzymes reached the values of most active natural catalysts of Kemp reaction, between 0.018 – 1.37 s^{-1}. Authors suggest that the lack of flexibility of the construct is a major shortcoming of their design, as it weakens the substrate and transition-state binding affinity.

We proposed an approach to use the essential elements of the protein's active site, as a starting point to design a highly precise, DNA-based nanodevice capable of *in situ* and *de novo* recreation of the original catalytic properties. The majority of the available software packages for modelling of DNA-based nanostructures are built on the underlying premise that if elements of the nanostructure are in the steric and electrostatic energy minimum, the structure as a whole would be, as well, close to its local minimum of potential energy. In experiments, this would mean a higher probability for the correctly folded nanostructure to be observed, as proven to work in the design and fabrication of various DNA-origami nanostructures [15-18]. As the conformational possibilities of the non-DNA elements of the nanostructure are harder to predict with certainty, we implemented the same premise in designing of the emulated catalytic site. For this reason, the quality of the structural, phylogenetic and kinetic data, with the extent and complexity of the molecular dynamics simulations, were of paramount importance during the design process of the D-SEPEC. In contrast to the Shell and Carrier Strands, the active centre of the D-SEPEC was created to be a conformational flexible structure, where the fluctuation of residues would resemble the structure capable of the active catalysis, only in a certain percentage of time.

We demonstrated how to measure and quantify the catalytic activity, and how to recycle and re-use nanodevices in multiple experiments. We separated the nanodevice into logical elements and tested their combinations for the ability to hydrolyse an ATP substrate. We designed experiments to activate and inactivate the catalytic potential and to locate its molecular origin. As the interactions between the DNA based nanostructures and Malachite Green reagent let to the aggregation and precipitation with significant influence on the measurements, we developed a product separation system based on the ultrafiltration, which allowed for reliable results with relatively small deviations in replicate measurements. We successfully staled the reactions by heat denaturation, and by the removal of the essential POC molecules from the otherwise correctly built Shell and Carrier structure. By doing so, we observed that the correct assembly of the D-SEPEC plays a major role in the emulation of the catalytic activity, as only correctly positioned POC molecules would maintain the turnover speed of the reaction. Further evidence was provided with the low product accumulation in the control reactions made of randomly interacting POC molecules, even in the 5 times higher concentration.

In our experiments, the concentration of the nanostructures in each reaction was approximated to 1 nm. As the concentration was determined as the maximum possible concentration for the measured amount of DNA in the sample, it is reasonable to assume that the real concentration of the fully assembled D-SEPEC nanostructures might be significantly lower. This is important to note, as the lower percentage of the properly assembled nanodevices would mean equally higher turnover rate of the individual unit. Further, as we have shown in the heat denaturation experiments, misfolded and aggregated DNA-based nanostructures would still retain the background product generation inherent to the DNA, which makes the corrected turnover speed of the D-SEPEC lower than in the reality (Fig. 2).

By taking into account the turnover speed (k_{cat} = 0.2271 – 0.3622 s^{-1}) observed in the reactions of the functional D-SEPEC nanostructure, that are *on par* to the native FlaI enzyme, we can conclude that the further improvements to this technology would lead to the substantial advances in the field of artificial enzymes and nanotechnology. Implementation of this approach, to the enzymes of extremely conserved secondary structure and rapid turnover rates could prove beneficial for development of new diagnostic tools, while emulation of the slow or hard to purify enzymes could open new possibilities in the fields of chemical industry.

MATERIALS AND METHODS

Molecular dynamics and structural phylogenetic analysis of the FlaI protein complex:

The crystal structure of the FlaI *Sulfolobus acidocaldarius* was used to construct the *in silico* systems of the FlaI monomers, dimers and hexamers, both with and without substrates in their active sites. All-atom molecular dynamics of the systems were simulated with the trajectory length of up to 200 ns. All systems were simulated and analysed using the program packages GROMACS, AMBER, SCHRODINGER and VMD [39 – 42]. The protein sequences of the 20 FlaI homologues from the available species, with sequence similarity above 90%, were compared and analysed using the BLOSUM62 pairwise alignment method. The variation scores were mapped on the structure of the *Sulfolobus acidocaldarius FlaI* protein, obtained by the MD simulations, using the MAESTRO programme package [41].

Self-assembly and purification of the Shell elements, and super-assembly of the D-SEPEC nanodevice:

The fabrication of D-SEPEC nanodevices was carried out in sequence, following the accepted guidelines on the assembly of DNA-origami based nanostructures [43]. The self-assembly was conducted in the Assembly buffer, under neutral pH and high salt environment (50 mM TRIS buffer, 18 mM MgCl2, pH=7.0). The folding reactions of each Shell element were PEG purified by the

method reported by Stahl et al. (2014) using the PEG precipitation buffer (15% (w/v) PEG-8000, 5 mM Tris, 505 mM NaCl) [43]. The super assembly was done by pooling the equimolar concentrations of preassembled Shell elements with the five times higher concentration of Carrier strands and POC elements, under the high salt concentration/neutral pH assembly conditions (50 mM TRIS buffer, 18 mM MgCl2, pH=7.0). The pooled elements where incubated over 48 hours using the temperature gradient from 60 °C to the RT, with temperature drop of 1 °C every 45 minutes.

Agarose gel electrophoresis (AGE) and concentration measurment of nanostructures:

The samples were mixed with 1/4× of DNA gel loading dye (6x) and loaded into a 2% agarose gel in 0.5× TAE buffer and runned for 3-3.5 hrs at 70 v. Both the agarose gel and the buffer contain 11 mM MgCl2. The electrophoresed agarose gels were stained with SYBER Safe and scanned using UVP scanner.

Negative staining transmission electron microscopy (nsTEM):

The morphological examination of nanostructures was done using transmission electron microscope (TEM) performed on a Morgagni operated at 80 kV. The images were taken by a Morada camera. Samples were prepared by dropping 5 µl of diluted nanostructures on glow-discharged carbon-coated Cu400 TEM grid and negative staining using 2% Uranyl acetate.

Catalytic activity assay and product separation

Test and control reaction samples were subjected to the range of substrate concentration (0, 25 and 50 uM ATP) and incubation times (0, 6, 12, 18 and 24h). The reaction buffers in all samples were maintained under the neutral pH and high salt conditions (50 mM TRIS buffer, 18 mM MgCl2, pH=7.0). Concentration of all nanostructures involved in the experiments was 1 nM. Concentration of POC and Filler pools elements was 5 nM. Following the incubation, generated product was separated from the nanostructures on the ultrafiltration columns (15 000 g, 15 min, 5kDa pores, Amicon). The flow through samples were transferred to the white, non-binding, clear bottom, plate wells (Greiner Bio-one, fisher scientific), containing malachite green reagent. Samples were quickly mixed and measured by using the high resolution spectroscopy (EnSpire, PerkinElmer). Measured wavelength was 624 nm, with each sample measured 10 times over several seconds.

Recycling of the nanostructures

The DNA nanostructures retained in the ultrafiltration reservoir was immediately reused, by ultra-filtrating each sample in 500 µl of the Assembly buffer. The ultrafiltration removed the leftover traces of ATP, ADP and PO_4^3. To initiate the next experiment samples were diluted to their original concentration, using the 50 ul of the Assembly buffer (50 mM TRIS buffer, 18 mM MgCl2, pH=7.0) with added correct amounts of the substrate.

ACKNOWLEDGMENTS

This project has received funding from the European Union's Horizon 2020 research and innovation program under grant agreement No. 686647

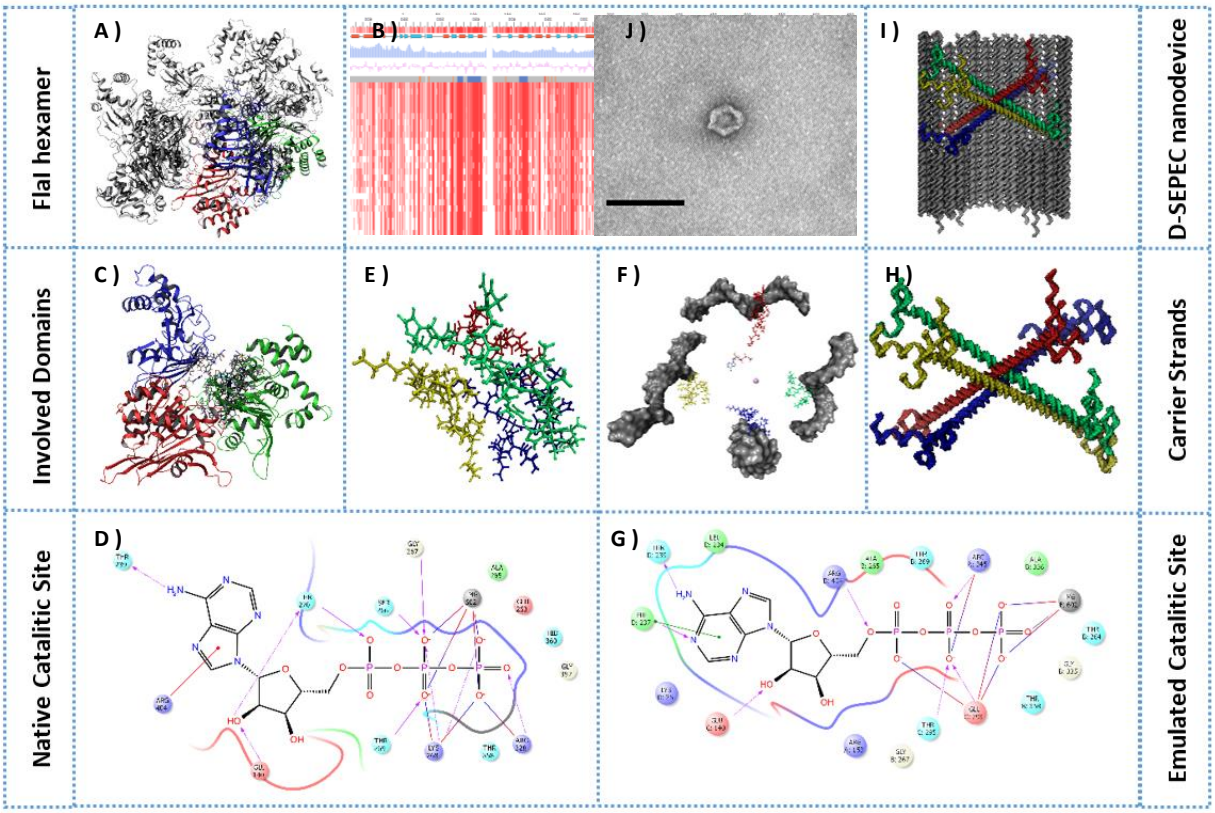

Figure 1. Pipeline for a design of the D-SEPEC nanodevice based on the FlaI protein complex. A) Structure of the FlaI hexamer obtained after 200 ns of the molecular dynamics simulation. Each active site is composed from the residues of 2 neighbouring FlaI monomers, with significant deviations of relative domain positions. Three involved domains are coloured in red, blue and green; B) Multiple alignment of the available sequences with 90% sequence similarity to the FlaI from the *S. acidocaldarius;* C) Structure of isolated domains involved in one of the active sites of the FlaI hexamer, with mapped conserved amino acids. D) 2D-representation of the interactions between residues of active site of the native FlaI protein and the ATP substrate; E) Peptide elements model from the key amino acids of the FlaI's active site. In recursive process, residues were added and connected to the key amino acids, until four peptides, 10 to 15 amino acids in length were formed; F) Divided structures of the POC elements of the D-SEPEC; G) 2D representation of the interactions between POC elements of the emulated catalytic site; H) Model of the POC elements integrated into the Carrier strands with ends prolonged into the staple strands of the Shell structure; I) Structure of the fully assembled D-SEPEC nanodevice. Structure can be separated into the groups of elements: hexagonal Shell superstructure; linear Carrier strands embedded under the precise angles on the Shell; and the set of peptide-oligonucleotide conjugates that form an emulated active site. J) Structural integrity of the Shell structure confirmed by a TEM imaging. Scale bar represents 100 nm.

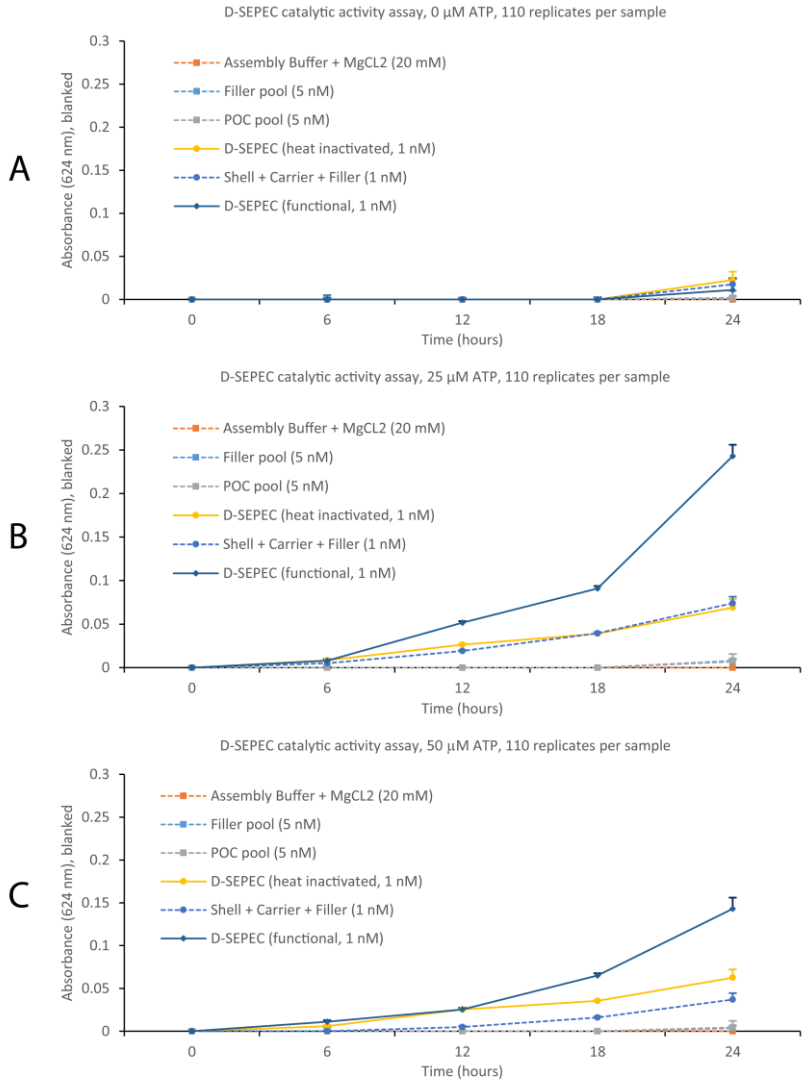

Figure 2. Product formation was measured by a high-resolution spectroscopy, in discrete time intervals, using the malachite green assay. Catalytic activity was measured under 0 (A), 25 µM (B) and 50 µM (C) concentration of the substrate. To remove influence of the autohydrolisation of the ATP, samples were blanked by the values of control samples with the Assembly buffer and $MgCl_2$, under same conditions and substrate concentrations. Heat inactivation of the functional D-SEPEC nanodevice (yellow) is marked by a significant drop in accumulation of PO_4^{3-}, close to the levels observed from non-functional structure of Shell, Carrier and Filler elements (blue, dotted). Samples of D-SEPEC nanodevice exhibited strongest increase of the product generation with k_{cat} values of 0.2271 s^{-1} in systems incubated with 25 µM of ATP, and 0.3622 s^{-1} in systems with 50 µM of ATP.

REFERENCES AND NOTES

1. A. Amit *et al.*, An antioxidant nanozyme that uncovers the cytoprotective potential of vanadia nanowires. Nature Commun. 5, 5301 (2014). doi: 10.1038/ncomms6301
2. Linko, V. *et al.*, A modular DNA origami-based enzyme cascade nanoreactor. Chem. Commun. 51, 5351–5354 (2015). doi: 10.1039/C4CC08472A
3. M. Liu *et al.*, A DNA tweezer-actuated enzyme nanoreactor. Nature Commun. 4, 2127 (2013). doi: 10.1038/ncomms3127
4. A. S. Walsh *et al.*, DNA Cage Delivery to Mammalian Cells. ACS Nano 5, 5427-32 (2011). doi: 10.1021/nn2005574
5. M. D. E. Jepsen *et al.*, Development of a genetically encodable FRET system using fluorescent RNA aptamers. Nature Commun. 9, 18 (2018). doi: 10.1038/s41467-017-02435-x
6. Y. Choi *et al.,* DNA Origami-Based Förster Resonance Energy-Transfer Nanoarrays and Their Application as Ratiometric Sensors. ACS Appl.Mater. Interfaces 10, 23295-23302 (2018). doi: 10.1021/acsami.8b03585
7. C. Wu *et al.,* Building a Multifunctional Aptamer-Based DNA Nanoassembly for Targeted Cancer Therapy. J.Am.Chem.Soc. 135, 18644-18650 (2013). doi: 10.1021/ja4094617
8. S. M. Douglas *et al.,* A Logic-Gated Nanorobot for Targeted Transport of Molecular Payloads. Science 335, 831-834 (2012). doi: 10.1126/science.1214081
9. Y. Choi *et al.,* A new reporter design based on DNA origami nanostructures for quantification of short oligonucleotides using microbead. Scientific Reports 9, 4769 (2019). doi: 10.1038/s41598-019-41136-x
10. F. Berger *et al.,* Regulation of poly(ADP-ribose) polymerase 1 activity by the phosphorylation state of the nuclear NAD biosynthetic enzyme NMN adenylyl transferase 1. Proc. Natl. Acad. Sci 104, 3765-70 (2007). doi: 10.1073/pnas.0609211104
11. X. Chang *et al.,* Role of N-linked glycosylation in the enzymatic properties of a thermophilic GH 10 xylanase from Aspergillus fumigatus expressed in Pichia pastoris. PLOS One (2017). doi: 10.1371/journal.pone.0171111
12. H. Lee *et al.,* Molecularly self-assembled nucleic acid nanoparticles for targeted in vivo siRNA delivery. Nature Nanotech. 7, 389-393 (2012). doi: 10.1038/nnano.2012.73
13. B. Wei *et al.,* Complex shapes self-assembled from single-stranded DNA tiles. Nature 486, 623-626 (2012). doi: 10.1038/nature11075
14. E. S. Andersen *et al.,* Self-assembly of a nanoscale DNA box with a controllable lid. Nature 459, 73-76 (2009). doi: 10.1038/nature07971
15. D. Han *et al.,* DNA Origami with Complex Curvatures in Three-Dimensional Space. Science 332, 342-346 (2011). doi: 10.1126/science.1202998
16. S. M. Douglas *et al.,* Rapid prototyping of 3D DNA-origami shapes with caDNAno. Nucleic Acids Res. 37, 5001-6 (2009). doi: 10.1093/nar/gkp436
17. D. N. Kim *et al.,* Quantitative prediction of 3D solution shape and flexibility of nucleic acid nanostructures. Nucleic Acids Res. 40, 2862-8 (2012). doi: 10.1093/nar/gkr1173
18. R. Veneziano *et al.,* Designer nanoscale DNA assemblies programmed from the top down. Science 352, 1534 (2016). doi: 10.1126/science.aaf4388
19. S. Reindl *et al.,* Insights into FlaI Functions in Archaeal Motor Assembly and Motility from Structures, Conformations, and Genetics. Mol. Cell. 49, 1069-82 (2013). doi: 10.1016/j.molcel.2013.01.014
20. D. Rothlisberger *et al.,* Kemp elimination catalysts by computational enzyme design. Nature 453, 190-195 (2008). doi: 10.1038/nature06879
21. D.W. Watkins *et al.,* Construction and in vivo assembly of a catalytically proficient and hyperthermostable de novo enzyme. Nature Commun. 8, 358 (2017). doi: 10.1038/s41467-017-00541-4
22. A. E. Donnelly *et al.,* A de novo enzyme catalyzes a life-sustaining reaction in Escherichia coli. Nat. Chem. Biol. 14, 253-255 (2018). doi: 10.1038/nchembio.2550
23. F. Richter *et al.,* De Novo Enzyme Design Using Rosetta3. PLOS One (2011). doi: 10.1371/journal.pone.0019230
24. M. D. Arifuzzaman, Y. Zhao, Artificial Zinc Enzymes with Fine-Tuned Catalytic Active Sites for Highly Selective Hydrolysis of Activated Esters. ACS Catal. 8, 8154-8161 (2018). doi: 10.1021/acscatal.8b02292
25. M. L. Romero *et al.,* Simple yet functional phosphate-loop proteins. PNAS 115, 11943-50 (2018). doi: 10.1073/pnas.1812400115
26. P. Chaudhury *et al.,* Characterization of the ATPase FlaI of the motor complex of the Pyrococcus furiosus archaellum and its interactions between the ATP-binding protein FlaH. Peer J. 6, 4984 (2018). doi: 10.7717/peerj.4984

27. P. Kosuri *et al.,* Rotation tracking of genome-processing enzymes using DNA origami rotors. Nature 572, 136 -140 (2019). doi: 10.1038/s41586-019-1397-7

27. A. E. Marras *et al.,* Programmable motion of DNA origami mechanisms. PNAS 112, 713-718 (2015). doi: 10.1073/pnas.1408869112
28. B. Repen *et al.,* Optimization of a malachite green assay for detection of ATP hydrolysis by solubilized membrane proteins. Anal. Biochem. 15, 103-5 (2012). doi: 10.1016/j.ab.2012.04.016

29. H. Takahashi *et al.,* Drastic Compensation of Electronic and Solvation Effects on ATP Hydrolysis Revealed through Large-Scale QM/MM Simulations Combined with a Theory of Solutions. J. Phys. Chem. B 121, 2279-2287 (2017). doi: 10.1021/acs.jpcb.7b00637
30. C. B. Harrison, K. Schulten, Quantum and classical dynamics simulations of ATP hydrolysis in solution. J. Chem. Theory. Comput. 8, 2328-2335 (2012). doi: 10.1021/ct200886j
31. M. Priess *et al.,* Molecular Mechanism of ATP Hydrolysis in an ABC Transporter. ACS Cent. Sci. 4, 1334-1343 (2018). doi: 10.1021/acscentsci.8b00369
32. M. Dittrich *et al.,* On the Mechanism of ATP Hydrolysis in F1-ATPase. Biophys. J. 85, 2253-2266 (2003). doi: 10.1016/S0006-3495(03)74650-5
33. F. A. Kiani, S. Fischer, Comparing the catalytic strategy of ATP hydrolysis in biomolecular motors. Phys. Chem. Chem. Phys. 18, 20219-233 (2016). doi: 10.1039/C6CP01364C
34. O. I. Wilner *et al.,* Enzyme cascades activated on topologically programmed DNA scaffolds. Nature Nanotech. 4, 249-254 (2009). doi: doi.org/10.1038/nnano.2009.50
35. V. Linko *et al.,* A modular DNA origami-based enzyme cascade nanoreactor. Checm. Commun. 51, 5351 – 5354 (2015). doi: 10.1039/C4CC08472A
36. G. Grossi *et al.,* Control of enzyme reactions by a reconfigurable DNA nanovault. Nature Commun. 8, 992 (2017). doi: 10.1038/s41467-017-01072-8
37. F. Praetorius, H. Dietz, Self-assembly of genetically encoded DNA-protein hybrid nanoscale shapes. Science 355, 5488 (2017). doi: 10.1126/science.aam5488
38. M. J. Abraham *et al.,* GROMACS: High performance molecular simulations through multi-level parallelism from laptops to supercomputers. SoftwareX 1, 19-25 (2015). doi: 10.1016/j.softx.2015.06.001
39. D.A. Case *et al.* AMBER 2016, University of California, San Francisco (2016).
40. Schrödinger Release 2019-3: Maestro, Schrödinger, LLC, New York, NY, (2019).
41. W. Humphrey *et al.,* VMD: Visual molecular dynamics. J. of Mol. Graph. 14, 33-38 (1996). doi: 10.1016/0263-7855(96)00018-5
42. E. Stahl *et al.,* Facile and scalable preparation of pure and dense DNA origami solutions. Angew. Chem. Int. Ed. 53, 12735-40 (2014). doi: 10.1002/anie.201405991
43. R. Owczarzy *et al.,* IDT SciTools:a suite for analysis and design of nucleic acid oligomers. Nucleic Acids Res. 36, 163-169 (2008). doi: 10.1093/nar/gkn198